ISSN 0036-0244, Russian Journal of Physical Chemistry A, 2011, Vol. 85, No. 10, pp. 1679–1688. © Pleiades Publishing, Ltd., 2011.
Original Russian Text © A.N. Zakharov, A.F. Maiorova, A.N. Kharlanov, K.B. Kalmykov, 2011, published in Zhurnal Fizicheskoi Khimii, 2011, Vol. 85, No. 10, pp. 1805–1815.

CHEMICAL THERMODYNAMICS AND THERMOCHEMISTRY

Thermal and Spectral Features of Nickel Compounds Synthesized within the Pores of Photonic Crystals Based on SiO_2

A. N. Zakharov, A. F. Maiorova, A. N. Kharlanov, and K. B. Kalmykov

Department of Chemistry, Moscow State University, Moscow, 119991 Russia

e-mail: zakh-alex@yandex.ru

Received October 18, 2010

Abstract—Nanoparticles of $NiC_2O_4 \cdot 2H_2O$ were obtained within the interspheric voids of synthetic opal polycrystalline samples based on SiO_2. The thermal decomposition of $NiC_2O_4 \cdot 2H_2O$ inclusions within the pores of crystallites was studied by means of thermal gravimetry and differential scanning calorimetry under static conditions in atmospheres of He and air. The efficient activation energy of dehydration (180 ± 10 kJ mol^{-1}) and dehydration enthalpy of nickel oxalate crystalline hydrate (69.9 kJ mol^{-1}) within the pores of photonic crystals based on SiO_2 were calculated. Pyrolysis of the nickel oxalate led to the formation of NiO nanoparticles within the voids and on the external surface of the photonic crystallites. The behavior of polycrystalline samples of the photonic crystals in a medium of immersion liquids was studied. It was shown that the partial population of the interspheric pores of photonic crystals with $NiC_2O_4 \cdot 2H_2O$, NiO, and Ni that diffuse visible light do not lead to a total loss of light conductivity in the immersion medium. The diffuse reflection spectra of a sample of photonic crystals populated with $NiC_2O_4 \cdot 2H_2O$ and NiO phases were recorded. A sample of photonic crystals with inclusions of metallic nickel particles exhibiting magnetic properties was obtained by treating nickel oxide-containing synthetic opal based on SiO_2 with molecular hydrogen.

Keywords: nickel compounds, thermal properties, spectral features, efficient activation energy, immersion liquids, light conductivity.

DOI: 10.1134/S0036024411100335

INTRODUCTION

Transition metal compounds are often used for loading the voids of porous supports to prepare polyfunctional systems that exhibit new optical, magneto optical, catalytic, and other important properties. The mode of loading within pores depends on the host's phase structure, as do the shape and sizes of the inclusions themselves.

Special attention has recently been devoted to photonic crystals as indifferent phases, particularly synthetic opals based on SiO_2. These substances are of special interest, owing to the unique optic characteristics associated with their inner structures. Photonic crystals are effectively used in the production of certain kinds of light switches (optical transistors, microresonators, splitters, and filters), and in other areas that require the precision tuning of light streams.

At the same time, the properties of photonic crystals depend heavily on the presence of phases of other products within the interspheric voids modifying 3D lattices formed of closely-packed quasi-spheres of oligomeric silicon dioxide. The introduction of different inclusions into the pores of photonic crystals allows targeted modification of the support's characteristics, successfully combining its physical chemistry properties with features of the guest phases. Polycrystalline samples of photonic crystals populated with ferromagnetic phases of metallic iron and cobalt were thus obtained in [1, 2].

The aim of this work was to prepare and study the thermal and spectral properties of synthetic opal samples based on SiO_2 and populated with $NiC_2O_4 \cdot 2H_2O$, NiO, and Ni polycrystalline phases that diffuse and reflect visible light.

Photonic crystals based on SiO_2 are three-layered closely-packed FCCs of quasi-sphere polycondensed SiO_2 molecules with effective diameters of 250–300 nm. Figure 1 shows a microphotograph of a part of a sample surface of synthetic opal based on SiO_2, obtained by scanning electron microscopy (SEM). It can be seen that the spheres formed by polycondensed SiO_2 molecules are actually not ideal rigid spheres. The volume of the tetrahedric and octahedric voids drops (relative to an ideal FCC lattice) as a result of compression. Even in this case, however, the apparent sizes of the synthetic opal crystallites' interspheric voids are entirely suited to housing microphases of other substances with diameters of up to 20–30 nm.

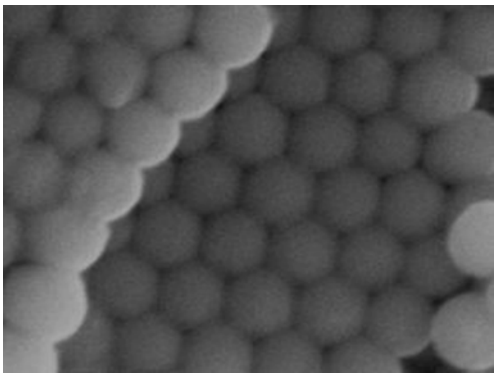

Fig. 1. Microphotograph of a surface fragment of a polycrystalline sample of photonic crystals based on SiO_2, obtained by scanning electron microscopy (SEM).

Inclusions of $NiC_2O_4 \cdot 2H_2O$(**I**) (a **I**/SiO_2 sample) were produced using the reaction between $NiCl_2$ and $H_2C_2O_4$, occluded within the interspheric voids of polycrystalline opal based on SiO_2. Subsequent thermal treatment of the **I**/SiO_2 yielded NiO inclusions (a **II**/SiO_2 sample). The reduction of **II**/SiO_2 in a molecular hydrogen atmosphere results in the in situ formation of a metallic nickel phase in the synthetic opal's pores (a **III**/SiO_2 sample).

EXPERIMENTAL

Diffuse reflection electronic spectra were recorded using an EQUINOX 55/S UV–VIS-spectrometer in the region of 300–900 nm at about ~20°C. The condition of the samples' surfaces was studied by SEM on an EVO-50 electron microscope (Zeiss) equipped with an EDX analyser.

The magnetic moments[1] were measured on a vibration magnetometer (magnetic moment sensibility, 8×10^{-11} A m^2) in the –800 + 800 kA/m region at about ~20°C. The sample vibrated within the poles of the electromagnet. The periods of vibrations were measured for each value of magnetic induction as it was varied discretely in small increments.

The thermal properties of the samples were studied using a Netzsch STA 409 thermal analyser under static conditions in He (without additional purification from residual oxygen) and in air at 300–700 K. The volume of the reaction chamber was 10 l. The temperature (T) was raised at a constant rate (β) according to the linear law $T = T_0 + \beta t$ (T_0 is the initial temperature; t is time).

Polycrystalline samples of synthetic opal based on SiO_2 were used in our study. Oxalic acid and $NiCl_2 \cdot 6H_2O$ were recrystallized from ethanol. Organic solvents (chloroform, acetone, ethanol) were distilled at atmospheric pressure.

A typical polycrystalline sample of synthetic opal based on SiO_2 ($2 \times 5 \times 5$ mm^3) was loaded into a boiling saturated solution (25 cm^3) of $NiCl_2 \cdot 6H_2O$ in ethanol and was decanted after refluxing for 5 h. The obtained sample, which contained occluded $NiCl_2 \cdot 6H_2O$, was dried in air at 370 K under lower pressure to remove the solvent.

The air-dried samples at 350 K of photonic crystal containing occluded nickel chloride were treated with a saturated solution of oxalic acid in boiling acetone for 1 h. The bright green solid was separated from the solution of oxalic acid and extracted with acetone to remove the excess of $H_2C_2O_4$ and soluble products of the reaction. The obtained **I**/SiO_2 sample was dried at 300 K for 5 h and calcined in an oven in air at 700 K for 1 h. A **II**A/SiO_2 sample was obtained after pyrolysis.

The **II**B/SiO_2 sample was synthesized in a similar fashion, except that the removal of excess ethanol and the drying in air were repeated twice after the voids of the support were filled with nickel chloride.

Polycrystalline **II**A/SiO_2 and **II**B/SiO_2 samples of photonic crystals filled with nickel oxide were reduced in a hydrogen flow at 600–700 K for 30–60 min. A **III**/SiO_2 sample containing metallic nickel inclusions was obtained after the reduction of NiO.

RESULTS AND DISCUSSION

Thermal properties. The decomposition of nickel oxalate dihydrate was studied in detail in [3–12]. The results of $NiC_2O_4 \cdot 2H_2O$ degradation were found to depend on the process conditions: the composition of the gas phase (vacuum, inert gas, air); the experimental regime (static or dynamic); the physical condition of the sample (its density, porosity, and so on); the thermal properties of the reagents and the products (their thermal capacities, thermal conductivities, and so on); and the sizes and shape of the particles resulting from the manner in which they were obtained.

It follows from the data in the literature [7] that the thermal decomposition of metal oxalates is preceded by a single-stage process of dehydration, regardless of the composition of the gas phase:

$$MC_2O_4 \cdot 2H_2O = MC_2O_4 + 2H_2O.$$

The result of the thermal decomposition of dehydrated oxalates depends on a number of factors. For the dehydrated oxalates of certain transition metals, two paths of thermal decomposition in an inert atmosphere are known; these are generalized by the equations [7, 12]

$$MC_2O_4 = M + 2CO_2, \quad (1)$$

$$MC_2O_4 = MO + CO_2 + CO, \quad (2)$$

where M = Fe^{2+}, Co^{2+}, Ni^{2+}, Cu^{2+}, Zn^{2+}, and others.

Although the nickel oxalate belongs to the category of salts that decompose according to (1), some authors [11] not exclude reaction (2) but even consider it to be the main reaction, since even in the total absence of traces of oxygen, the product of the polythermic

[1] Magnetic measurements were made by N.S. Perov.

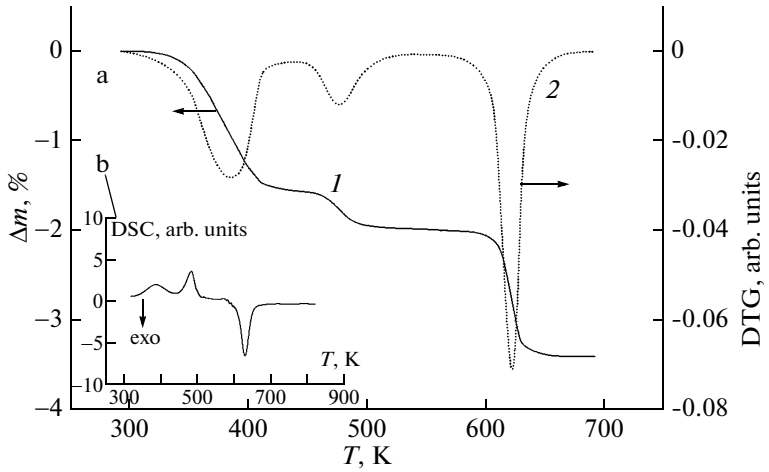

Fig. 2. Polythermic decomposition of $NiC_2O_4 \cdot 2H_2O$ inclusions within photonic crystals based on SiO_2 under static conditions in air at a heating rate of 2 K min^{-1}: (a) TG (*1*), DTG (*2*); (b) DSC; Δm is mass loss.

decomposition of $NiC_2O_4 \cdot 2H_2O$ always contains noticeable NiO impurities. These authors in this case explain the absence of CO in the gas phase by secondary reaction (3), which is in their opinion made easier by the spatial proximity of the CO and NiO oxides at the moment of gas evolution:

$$NiO + CO = Ni + CO_2. \quad (3)$$

True, it remains unclear why the C–O bond in the C–O–Ni oxalate group is initially broken and then reformed as a result of the more complex heterogeneous reaction between gaseous CO and solid NiO under dynamic conditions at a flow rate of 100 ml min^{-1}. On the other hand, the absence of CO in the gas phase ought to lead to a quantitative reduction of NiO, since CO and NiO are formed in equimolar ratio; this also does not agree with the experimental data. In addition, it is well known that more rigid conditions are required for NiO reduction by CO, relative to iron oxides. To obtain $Ni(CO)_4$ from nickel oxalate according to Mond [13], e.g., where a high degree of surface oxide purification is required, the product of the thermal decomposition of NiC_2O_4 is thus preliminarily treated with H_2 at 300–350°C.

Most of the researchers [3–11] who have studied the thermal properties of $NiC_2O_4 \cdot 2H_2O$ in an oxidizing atmosphere (oxygen, air) are of the opinion that nickel oxalate dihydrate is decomposed in two steps according to Eqs. (4) and (5), which reflect the appearance of endo- and exothermic effects, respectively:

$$NiC_2O_4 \cdot 2H_2O = NiC_2O_4 + 2H_2O, \quad (4)$$

$$NiC_2O_4 + (1/2)O_2 = NiO + 2CO_2. \quad (5)$$

At the same time, some researchers do not exclude the possibility that even in an oxidizing atmosphere, the second step (the decay of dehydrated NiC_2O_4) could be a superposition of two consecutive processes, i.e., the formation of metallic nickel grains according to an endothermic reaction of type (1) and an exothermic reaction of metallic nickel oxidation with atmospheric oxygen:

$$Ni + (1/2)O_2 = NiO. \quad (6)$$

The superposition of thermal effects opposite in sign at the pyrolysis stage of the dehydrated NiC_2O_4 thus explains the complex nature of the high-temperature exothermic peak.

There are no data in the literature on the thermal behavior of $NiC_2O_4 \cdot 2H_2O$ within the interspheric voids of photonic crystals, particularly those based on SiO_2, the features of whose pores impose certain limits on the size and shape of inclusions distributed over the support's cavity system in the form of nanoparticles with an average diameter of 20–30 nm.

We established that the composition of the gas phase (air or He containing residual oxygen) has virtually no effect the nature of the $NiC_2O_4 \cdot 2H_2O$ inclusions' thermal decay under static conditions. It does, however, considerably affect the behavior of nanoparticles within the pores of photonic crystallites, relative to the thermal properties of the free phase of $NiC_2O_4 \cdot 2H_2O$.

The typical thermal gravimetric (TG) trace its time derivative (DTG), and differential scanning calorimetry traces obtained at thermal treatment of the samples of the synthetic opal containing $NiC_2O_4 \cdot 2H_2O$ in air atmosphere are presented in Fig. 2. On the TG-trace obtained by the decomposition of $NiC_2O_4 \cdot 2H_2O$ within the pores of the support in air atmosphere were found: the low-temperature mass-loss change attributed to the removal of water adsorbed within pores of the photonic crystallites (353–410 K) and two mass loss changes connected with the dehydration of $NiC_2O_4 \cdot 2H_2O$ (458–490 K) and with the pyrolysis of the dehydrated nickel oxalate NiC_2O_4 (600–650 K), respectively.

Table 1. Polythermic decomposition of $NiC_2O_4 \cdot 2H_2O$ (**I**) in the free phase and in the form of microparticles within the pores of photonic crystallites based on SiO_2 (**I**/SiO_2) under static conditions in air and He. The heating rate is 2 K/min

Phase composition		m, mg		θ, %		ΔT, K	$\Delta m/m_0$, %		Δ_2/Δ_1	
A	B	m_0	m_1	TG	DSC		exp.	calcd.	exp.	calcd.
I/SiO_2	He	35.5	0.76	2.1	2.0	350–410	0.210	–	1.92	2.00
						430–463	0.42	0.40		
						615–632	0.81	0.78		
	Air*	14.56	0.37	2.54	2.5	353–410	1.52	–	2.62	2.55
						458–490	2.07	2.01		
						608–628	3.50	3.52		
I	He*	27.13	27.13	100	100	400–491	15.8	–	3.07	–
						578–601	51.38			
	Air*	13.2	13.2	100	100	452–513	20.60	19.67	2.82	3.01
						602–624	58.10	59.11		

Note: A and B are liquid and gas phases, respectively; m_1 is the $NiC_2O_4 \cdot 2H_2O$ mass in a sample with mass m_0; θ is the mass ratio of $NiC_2O_4 \cdot 2H_2O$ in a sample calculated according to the data of TG and DSC, respectively; m/m_0 is the relative mass loss of the sample during thermal decomposition of $NiC_2O_4 \cdot 2H_2O$ (**I**) and the thermal decomposition of **I** within the pores of photonic crystals (**I**/SiO_2); ΔT is the temperature region; Δ_1 and Δ_2 are the mass losses of the sample at the stages of $NiC_2O_4 \cdot 2H_2O$ dehydration and NiC_2O_4 thermal decomposition, respectively; the heating rate for the asterisked samples is 5 K/min.

Two consecutive endothermic effects and one exothermic effect were recorded on the DSC curves obtained upon the decomposition of $NiC_2O_4 \cdot 2H_2O$ in air within the pores of the photonic crystallites. The low-temperature endothermic effect attributed to the first mass-loss change is associated with the dehydration of the photonic crystals themselves, which agrees with the data obtained earlier for the polythermic decomposition of $CoC_2O_4 \cdot 2H_2O$ within the pores of synthetic opal based on SiO_2 [2]. The second endothermic effect at 430–490 K is due to the decomposition of $NiC_2O_4 \cdot 2H_2O$ crystal hydrate. The exothermic effect registered in the high-temperature region (608–632 K) of the decomposition of NiC_2O_4 is probably a superposition of thermal effects opposite in sign.

The same result is observed in an atmosphere of He containing residual oxygen. As in the case of free $NiC_2O_4 \cdot 2H_2O$ decomposition studied in an O_2 flow [11], the maximum of the decomposition temperature of NiC_2O_4 in air within the pores of the photonic crystals is shifted to the low-temperature region, relative to its position upon pyrolysis in He (Table 1).

The values of the mass losses due to the decomposition in air of $NiC_2O_4 \cdot 2H_2O$ within the voids of photonic crystallites correlate satisfactorily with the stoichiometry of reactions (4) and (5) (Table 1). In the high-temperature region, an exothermic effect is also registered upon the pyrolysis of dehydrated nickel oxalate in air within the pores of photonic crystallites; the nature of this effect is likely associated with similar processes that occur in the decomposition of free $NiC_2O_4 \cdot 2H_2O$.

On the DSC curve, however, as can be seen in Fig. 2, there is no split of the exothermic peak upon the pyrolysis of NiC_2O_4 nanoparticles within the pores of photonic crystals, as was observed earlier on the DTA curves for the polythermic decomposition of free NiC_2O_4 in a flow of O_2 [11]. Unfortunately, the authors could not explain this phenomenon and did not discuss it.

In some works, the complex nature of the exothermic effect registered at the temperatures of NiC_2O_4 pyrolysis in an oxidizing medium were explained in terms of a superposition of the endothermic effect of reaction (1) and certain exothermic effects attributed to secondary processes, e.g., the oxidation of metal nickel by oxygen (6), the reduction of nickel oxide (NiO) by CO (3), and the oxidation of CO by atmospheric oxygen:

$$CO + (1/2)O_2 = CO_2. \quad (7)$$

According to the data summarized in Table 1, the value of the mass loss corresponding to the exothermic effect of the polythermic decomposition of $NiC_2O_4 \cdot 2H_2O$ inclusions within photonic crystals based on SiO_2 agrees with Eq. (5), regardless of the composition of the gas phase (He, air). This indicates the formation of only one NiO compound in both cases. If He containing residual oxygen is replaced with air, however, the value of the specific exothermic effect increases; this is possible only if molecules of gaseous compounds participate in the exothermic process. The only gaseous compound that could react exothermically with oxygen is CO that forms upon the decomposition of NiC_2O_4 in accordance with Eq. (2). At the same time, it is well known that the burning of CO in air at atmospheric pressure is possible only at temperatures higher than 700°C. The exothermic effect is

thus probably associated with the heterogeneous catalytic oxidation of CO with atmospheric oxygen or the residual oxygen in the He. The quantity of the residual oxygen in the He is quite enough for the nickel's complete oxidation into NiO, due to the lower content of Ni in the photonic crystallites, relative to sample **I**. It is probably this effect that explains why there is no difference between the TG curves for the thermal decomposition of the $NiC_2O_4 \cdot 2H_2O$ within photonic crystallites in air and in He.

Some transition metals and their oxides exhibit noticeable activity in the heterogeneous catalytic oxidation of CO with atmospheric oxygen [14], though they are not, of course, as active as many known catalysts. Metals, oxides, and metal chelate compounds based on organic ligands deposited on solid supports (Al_2O_3, SiO_2, zeolites, etc.) are catalytically active in the CO oxidation reaction even upon moderate heating [2, 15]. We thus showed in [15], e.g., that the heterogeneous catalytic oxidation of CO with atmospheric oxygen on nickel and lanthanum oxides deposited on γ-Al_2O_3 already occurs in the temperature range of 420–570 K.

Moreover, it was established in [16] that the polythermic decomposition of $CoC_2O_4 \cdot 2H_2O$ within the pores of photonic crystals based on SiO_2 is also accompanied by an exothermic effect, due to the heterogeneous catalytic oxidation of CO masking the thermal effect of the endothermic reaction of the decomposition of dehydrated cobalt oxalate CoC_2O_4.

The observed exothermic effect corresponding to the high-temperature mass loss is thus likely to be composed of thermal effect of the decomposition of dehydrated nickel oxalate NiC_2O_4 nanoparticles in accordance with Eq. (2), and thermal effect of the heterogeneous catalytic oxidation of CO by oxygen over the forming phase of nickel oxide.

Under the same conditions, we used DSC to study the polythermic decomposition of free $NiC_2O_4 \cdot 2H_2O$. In Table 2, the results are compared to the data obtained for the **I**/SiO_2 sample. It follows from the data in Table 2 that the ratio of the decomposition heats of $NiC_2O_4 \cdot 2H_2O$ for the **I** and **I**/SiO_2 samples is 40.65, while the ratio of the corresponding thermal effects of the pyrolysis stage is 39.5. The coincidence of these values and their appreciable closeness to the ratio of the mass of $NiC_2O_4 \cdot 2H_2O$ in the initial **I** and **I**/SiO_2 samples (35.6) (Table 2) indicates the features of the polythermic decomposition of the free phase of $NiC_2O_4 \cdot 2H_2O$ after its loading in the form of nanoparticles into the pores of the photonic crystallites remain unchanged.

On the other hand, the ratios of the absolute values of the heat effects for the dehydration and pyrolysis stages of the polythermic decomposition of $NiC_2O_4 \cdot 2H_2O$ in air (Table 2), obtained empirically for the free and supported nickel oxalate, are also quite close within the range of experimental error: 1.69 and 1.74, respectively. The heat effect of reaction (4) was calculated on the basis of the data presented in Table 2 (69.9 ± 0.8 kJ mol^{-1}).

Table 2. Thermal effects observed for the polythermic heating of **I** and **I**/SiO_2 samples in air. The heating rate is 5 K/min

Sample	Mass, mg		ΔT, K	Q, J/g
	m_0	m_1		
I	27.13	27.13	452–513	400
			602–624	–676
I/SiO_2	14.56	0.37	353–410	23.1
			458–490	9.84
			608–628	–17.1

Note: m_1 is the $NiC_2O_4 \cdot 2H_2O$ mass in the corresponding sample; m_0 is the total mass of the sample; ΔT is the temperature region; and Q is the thermal effect.

The efficient activation energy of the dehydration of inclusions of $NiC_2O_4 \cdot 2H_2O$ for steady-state decomposition within the voids of photonic crystallites based on SiO_2 was estimated using the DSC data (180 ± 10 kJ mol^{-1}). This value is in good agreement with the efficient activation energy calculated earlier for the dehydration of free $NiC_2O_4 \cdot 2H_2O$ in a vacuum (210 kJ mol^{-1} [17]).

Behavior of the samples in immersion liquid. An interesting feature of photonic crystals based on SiO_2 loaded with the phases of $NiC_2O_4 \cdot 2H_2O$, NiO, and Ni was observed in immersion liquids (e.g., water, chloroform, acetone, and ethanol). Synthetic opals based on SiO_2 are known to be photonic conductors in an immersion liquid medium; in air, being photonic dielectrics, they diffuse visible light, as is illustrated by the example of an initial polycrystalline sample of a photonic crystal based on SiO_2 (Fig. 3).

The transparency of the samples of synthetic opals based on SiO_2 in a medium of immersion liquid is the same even after they are loaded with nickel compounds, e.g., with nickel chloride (the nickel oxalate precursor), which is retained in the solid phase due to occlusion after impregnation with ethanol or aqueous solutions of $NiCl_2 \cdot 6H_2O$. In acetone (which does not dissolve and thus does not extract the nickel chloride from the pores of the solid phase), the sample containing occluded $NiCl_2 \cdot 6H_2O$ was also transparent even after the maximum loading of interspheric voids. Subsequent treatment of a sample containing 1 wt % of $NiCl_2 \cdot 6H_2O$ with saturated solution of oxalic acid in acetone, however, led to virtually no reduction in transparency for visible light, though this procedure did result in the formation of new compound within the pores of the crystallites: nickel oxalate $NiC_2O_4 \cdot 2H_2O$, which effectively diffuses visible light in the amorphous or polycrystalline states.

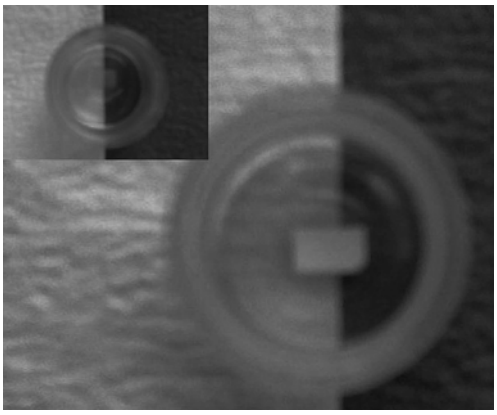

Fig. 3. Polycrystalline sample of photonic crystals based on SiO_2 in air (in center) and in a medium of immersion liquid (ethanol) (at upper left).

The interaction of reagents upon synthesis usually occurs mainly in the external layers of a solid in contact with the solution, so that the crystallite surface is enriched with the product of the reaction. In order to lower the possibility of the redistribution of nanoparticles containing nickel and to prevent its concentration within the external layers, the reaction with oxalic acid was performed in a solution of acetone. The occluded $NiCl_2 \cdot 6H_2O$ is insoluble in acetone, and the formation of nickel oxalate during impregnation with solution of oxalic acid in acetone occurred only on sites of nickel chloride localization. The migration of nickel chloride throughout the pores of the photonic crystallites while wetting with solvent was thus precluded. There was also no enrichment of the external layers of the solid phase with the product of the $NiC_2O_4 \cdot 2H_2O$ reaction.

Due to its extremely low solubility, the nickel oxalate synthesized within the pores of the matrix was not extractable from the photonic crystallites with either water or organic solvents. The nickel oxalate could be removed from the pores of the support only via the chemical decomposition of the inclusions, e.g., through treatment with mineral acids or complexing agents. The impossibility of $NiC_2O_4 \cdot 2H_2O$ migrating throughout the pores of synthetic opal impregnated with solvent fundamentally distinguishes this compound from its precursor, $NiCl_2 \cdot 6H_2O$, which can be completely removed from the solid by water or ethanol.

The optical properties of the matrix depend not only on the nature of the inclusions populating the voids of the support but also on the number of inclusions. No changes in the transparency of the samples containing $NiC_2O_4 \cdot 2H_2O$ in immerse liquids are observed until ~20–25% of the support is covered. An increase in the $NiC_2O_4 \cdot 2H_2O$ content leads to a total loss of the sample's transparency after wetting with solvent. The enhanced loading of the pores of the synthetic opal with nickel oxalate using the above multiple procedures results in intensive diffusion of light by the sample and finally in the total loss of transparency by wetting with solvent.

For visible light, the opacity of samples of opal based on SiO_2 is thus observed in an immersion liquid when there is a rather high content of inclusions of the polycrystalline micro phase of $NiC_2O_4 \cdot 2H_2O$ within the pores of the support. Not only are the optical features and concentration of the inclusions themselves of vital importance for the optical properties of a matrix populated with foreign phases, the nature of the microparticles' distribution over the voids and surface is important as well.

The samples of opal matrix based on SiO_2 containing $NiC_2O_4 \cdot 2H_2O$ inclusions within interspheric voids (and partially on the external surface of the crystallites) are light green, which is typical for this inclusion compound. After thermal treatment in air, leading to the formation of NiO within the pores of crystallites, the albedo and color of the sample change drastically. The lusterless face of the initial sample becomes metallically lustrous in air. The mirror-like face of the sample is indicative of the modification of the external layers of crystallites with nickel oxide particles, the sizes (h) of which must in this case satisfy the condition $h \ll \lambda$ (where λ is the wavelength of incident light). It is believed that there is mirror-like reflection of light when $h \leq 0.003\lambda$. The mirror-like reflection of visible light (400–800 nm) thus occurs when there are NiO particles with diameters of 15–30 nm on the surface of a **II**/SiO_2 sample.

The high albedo of the **II**/SiO_2 sample for incident light does not imply that the surface is absolutely smooth. In fact, the surface has a microrelief from irregularities of finite height that produce a stochastic diffusion of light. The reflection of light from the **II**/SiO_2 sample is therefore likely to be of a mixed character, and some part of the incident light is reflected diffusively. The features of the distribution of reflected light when there are NiO particles larger than the wavelength of the incident light ($h \geq \lambda$) that are regularly distributed over the surface of the **II**/SiO_2 sample (e.g., near interspheric voids) are similar to those of the reflection from a diffraction grating. The distance between inclusion nanoparticles on the surface of the material is also of great importance for interaction with light.

By analogy with the light green sample containing nickel oxalate inclusions, after calcination of the **I**/SiO_2 sample in air we might expect the new **II**/SiO_2 sample to be the greyish-green color typical of NiO. The color of the obtained samples, however, appeared to depend substantially on the surface concentration and dimensions of the NiO particles. We prepared samples containing 0.22 and 1.1 wt % of NiO (**II**A/SiO_2 and **II**B/SiO_2, respectively) that were given additional color. The **II**A/SiO_2 sample was thus red, while the more concentrated **II**B/SiO_2 sample was green.

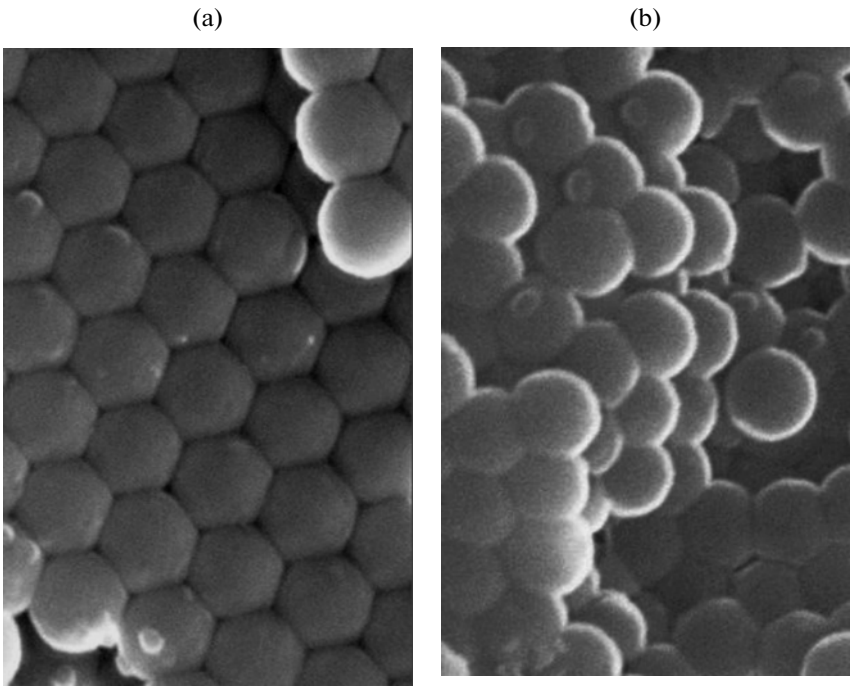

Fig. 4. Microphotographs of the surface of (a) polycrystalline **II**A/SiO_2 samples and (b) **II**B/SiO_2 of photonic crystals based on SiO_2 after thermal decomposition (in air) of $NiC_2O_4 \cdot 2H_2O$ inclusions obtained within interspheric voids.

Figure 4 shows SEM microphotographs of both samples. We can see the difference in the shape and nature of the distribution of the NiO particles on the surface. The microphotograph of **II**A/SiO_2 sample with less NiO shows ordered and well shaped spheric inclusions 20–30 nm in size. The **II**B/SiO_2 sample was obtained by higher loading of the support. Its face also reflects incident light like a mirror. We can see that there are more NiO particles on the surface of the green sample. Nevertheless, the NiO inclusions are close to pseudospheric in shape and there are no agglomerations on the surface.

Mild etching of the **II**B/SiO_2 sample with ammonia solution does not lead to a lower albedo, but the spectrum of the reflected light changes drastically due to a bathochromic shift of the absorption band. The spectral range of the reflected light is thus associated with the sizes and distribution of the NiO inclusions on the face of the sample, and the bathochromic shift of the maximum of the reflected light bands is a result of a change in the sizes of the NiO nanoparticles forming the superlattice.

Nanolocalization of light along a metal–dielectric boundary is a well-known phenomenon in which the energy of an optical wave is transferred to a subsystem of superficial plasmons. This phenomenon has been dubbed superficial plasmonic resonance and is now widely used in the production of optical nanomaterials in which heterogeneity in nanosizes lead to substantial changes in optical properties.

Optical superficial plasmonic polaritons also appear at the boundary between a metal-like phase (e.g., oxides) and a dielectric. The dependence of the optical properties of **II**A/SiO_2 and **II**B/SiO_2 samples containing NiO inclusions on the quantity of metal in photonic crystals clearly indicates the presence of NiO nanoparticles on the material surface.

Samples containing visibly opaque NiO inclusions also remain capable of transmitting visible light in an immersion liquid within a quite wide range of support void filling. As an example, Fig. 5 shows a microphotograph of **II**A/SiO_2 sample in a medium of immersion liquid (acetone).

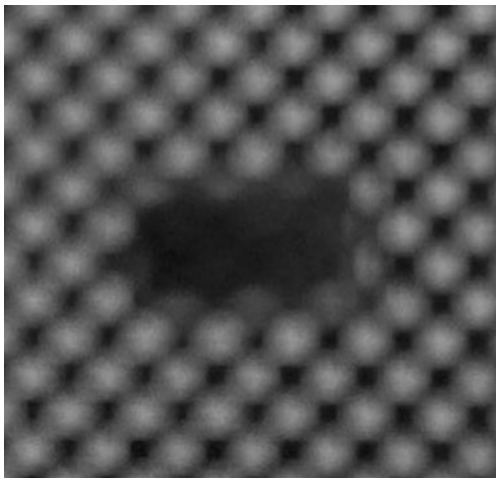

Fig. 5. Picture of **II**A/SiO_2 sample in a medium of immersion liquid (acetone).

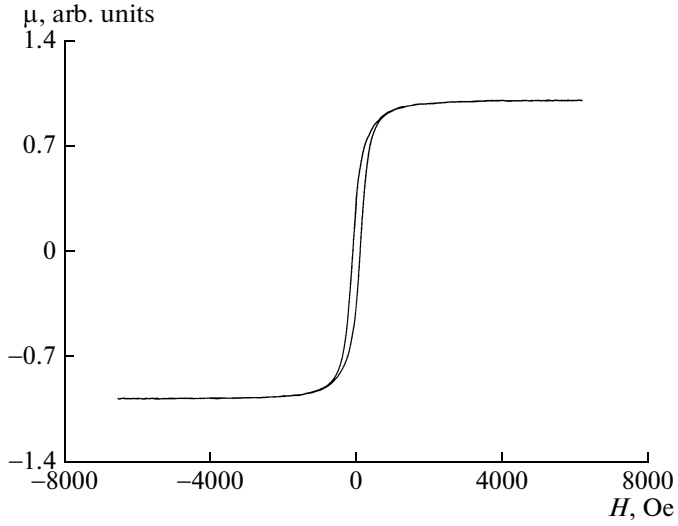

Fig. 6. Magnetization of a polycrystalline sample of synthetic opal based on SiO_2 and containing inclusions of metallic nickel at ~20°C; μ is the magnetic moment, and H is the magnetic field.

tograph of a **II**A/SiO_2 sample loaded with nickel oxide and immersed in acetone. We can see that the **II**A/SiO_2 sample retains the property of optical transmission in acetone, even though its voids are filled with optically opaque NiO phase. In the absence of solvent (i.e., in air), the **II**A/SiO_2 sample is absolutely opaque.

Reduction of the **II**A/SiO_2 and **II**B/SiO_2 samples with molecular hydrogen at 600–700 K leads to the formation of metallic nickel nanoparticles. The samples are almost indistinguishable externally and are black with a green tint. Samples thus obtained remain transparent to light in an immersion liquid at Ni loadings of up to 10% of the volume of the voids.

Magnetic and spectral properties. Polycrystalline **II**A/SiO_2 and **II**B/SiO_2 samples of synthetic opal based on SiO_2 containing NiO inclusions are nonmagnetic in –6000 ... +6000 Oe fields at room temperature. The high albedo of these samples with regard to visible light therefore cannot be due to the layer of metallic Ni particles formed after calcination of a sample containing $NiC_2O_4 \cdot 2H_2O$ inclusions.

Both samples become magnetic after reduction with molecular hydrogen in an inert atmosphere, which is indicative of the formation of metallic nickel inclusions. Figure 6 shows the dependence of **II**B/SiO_2 magnetization on the magnetic field. The hysteresis loop typical of ferromagnetics indicates that the sample contains a magnetically ordered phase. The coercive force values calculated for both **III**/SiO_2 samples are close: $H_c = 90$ Oe.

There are some peculiarities in the diffuse reflection spectra (DRSes) of polycrystalline samples of opal based on SiO_2 and modified with nickel oxalate, nickel oxide, and metallic nickel (Figs. 7–9). Figure 7 shows the absorption spectra of the initial polycrystalline synthetic opal based on SiO_2 and a sample with $NiC_2O_4 \cdot 2H_2O$ inclusions. A characteristic band attributed to electron transitions in the Ni^{2+} ions of the **I**/SiO_2 sample appears at 495 nm.

It should be noted that the position and intensity of the band in the DRSes of the **I**/SiO_2 sample at 495 nm are independent of the angle of incidence of the light

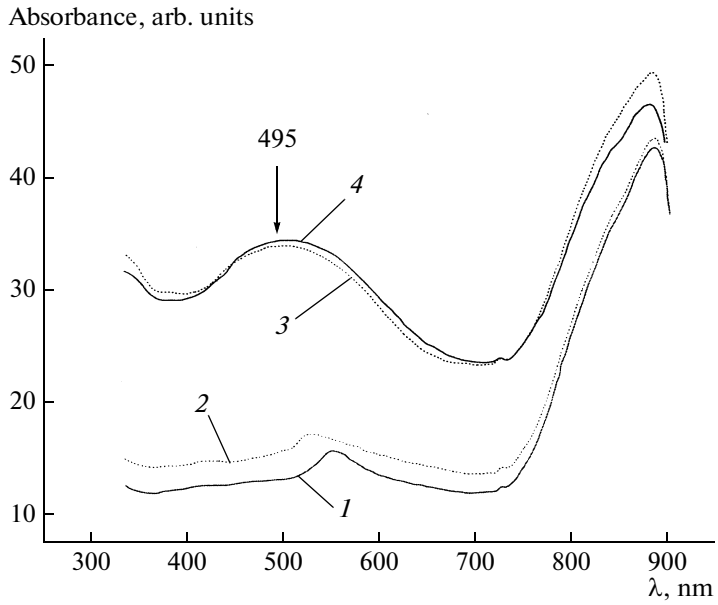

Fig. 7. Diffuse reflection spectra of polycrystalline samples of photonic crystals based on SiO_2 without inclusions (*1*, *2*) and containing $NiC_2O_4 \cdot 2H_2O$ inclusions (*3*, *4*). Light ray sliding angles: (*1*, *3*) 0°; (*2*, *4*) 45°.

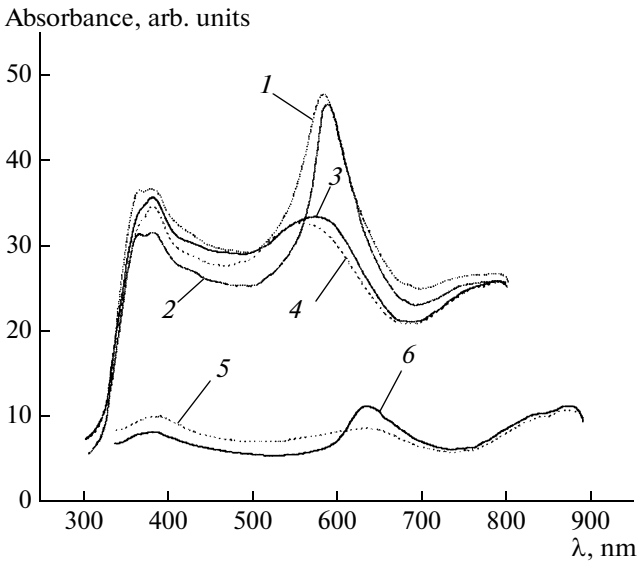

Fig. 8. Diffuse reflection spectra of polycrystalline **II**A/SiO_2 and **III**/SiO_2 samples of photonic crystals based on SiO_2 containing NiO inclusions. Light ray light sliding angles: (*1*) 0°; (*2*) 90°; (*3*) 45°; (*4*) 135°. For nanoparticles of metallic nickel: light ray sliding angles (*5*) 0°; (*6*) 45°.

rays, indicating its chemical origin due to *d-d* transitions of Ni^{2+} ions in the octahedral field of the donor oxygen atoms in the oxalate anions and water molecules. This band disappears at 495 nm completely after the thermal decomposition of the nickel oxalate inclusions, but two new bands appear simultaneously (Figs. 8 and 9) in the DRSes of the **II**A/SiO_2 and **II**B/SiO_2 samples. The positions of the bands are dependent not only on the degree to which the samples are covered with NiO inclusions but also on the light's angle of incidence. The higher frequency band is thus recorded at 394 nm in DRSes of the **II**A/SiO_2 sample poorer in NiO, and it appears at 368 nm in the DRSes of the **II**B/SiO_2 sample richer in NiO.

The behavior of the higher frequency band recorded in DRSes of the **II**B/SiO_2 sample in dependence on the light's angle of incidence is noteworthy: it appears only when the angle of incidence is perpendicular to the surface (sliding angle, 90°). At a 45° angle of incidence, the higher frequency band is not registered. In the case of the **II**A/SiO_2 sample, this band is recorded at both angles of incidence, and its position and intensity are unchanged.

There is a notable difference between the positions of the lower frequency bands in DRSes of the **II**A/SiO_2 and **II**B/SiO_2 samples. The lower frequency band is shifted to the high frequency region at 80–90 nm upon an increase in the NiO content of synthetic opal based on SiO_2, which explains the change in the color of the sample. At the same time, the intensity of the lower frequency band, like that of the higher frequency band, depends on the light's angle of incidence as well. The intensity of this band increases dramatically for both samples as the angle of incidence grows from 0° to 45° (Fig. 7).

The spectral properties of synthetic opal with NiO inclusions also change after reduction with molecular

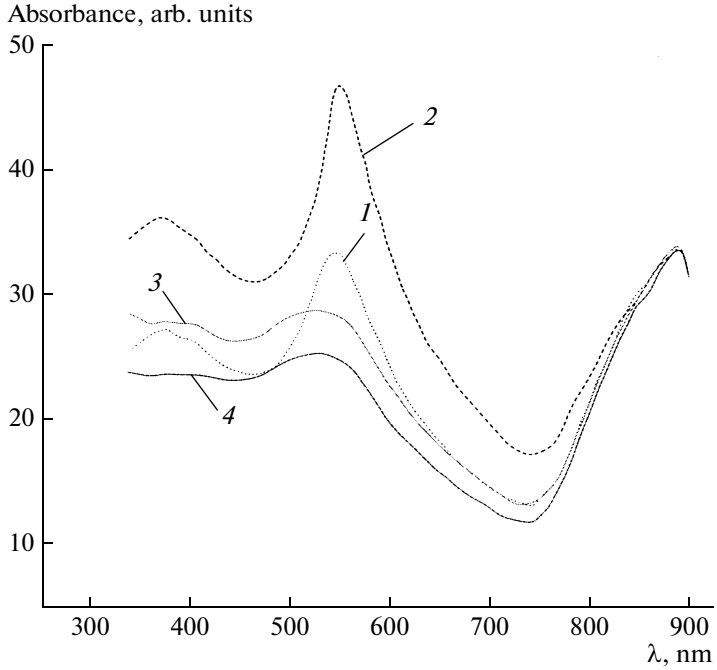

Fig. 9. Diffuse reflection spectra of polycrystalline **II**B/SiO_2 samples of photonic crystals based on SiO_2 containing NiO inclusions. Light ray sliding angles: (*1*) 0°; (*2*) 90°; (*3*) 45°; (*4*) 135°.

hydrogen at 600–700 K. Figure 8 presents DRSes for **III**/SiO_2 obtained after reduction of nickel oxide inclusions with molecular hydrogen. The character and position of the bands for the sample containing metallic nickel are virtually unchanged, but the intensity of the bands falls drastically.

CONCLUSIONS

Synthetic opals based on SiO_2 populated with $NiC_2O_4 \cdot 2H_2O$, NiO, and Ni thus not only retain the unique optical features of photonic crystals themselves but also allow their deliberate modification by changing the nature of the inclusions filling the interspheric pores. On the other hand, the inclusions enable us to change the optical properties of the surface of samples, via the formation of a second superlattice that leads to the appearance of superficial polaritonic waves. At the same time, samples of photonic crystals doped with magnetically ordered phases become magnetic due to magnetically ordered inclusions. The above features and unique properties of synthesized **I**/SiO_2–**III**/SiO_2 samples lead us to believe they will be studied further in different branches of science, and be applied effectively in technology.

REFERENCES

1. A. N. Zakharov, E. A. Gan'shina, N. S. Perov, et al., Izv. RAN, Neorg. Mater., No. 11, 1343 (2005).
2. A. N. Zakharov, A. F. Maiorova, M. L. Kovba, and M. A. Bykov, Zh. Fiz. Khim. **84**, 538 (2010) [Russ. J. Phys. Chem. A **84**, 466 (2010)].
3. E. Bircumshaw, J. Chem. Soc., p. 1800 (1950).
4. A. Scaife, J. Phys. Chem. **58**, 667 (1954).
5. G. M. Zhabrova, B. M. Kadenatsi, N. B. Zvonov, et al., Kinet. Katal. **3**, 610 (1962).
6. D. Dollimore, Thermochim. Acta **117**, 331 (1987).
7. V. A. Sharov, V. A. Zhilyaev, E. A. Nikonenko, and T. M. Zhdanovskikh, Koord. Khim. **6**, 431 (1980).
8. D. Dollimore, G. R. Heal, and R. W. Krupay, Thermochim. Acta **24**, 293 (1978).
9. V. Danesh, Probl. Kinet. Katal. **10**, 450 (1960).
10. D. Broadbent, D. Dollimore, and J. Dollimore, J. Chem. Soc. A, 278 (1966).
11. E. D. Macklen, J. Inorg. Nucl. Chem. **30**, 2689 (1968).
12. V. P. Kornienko, Ukr. Khim. Zh. **23**, 159 (1957).
13. V. G. Syrkin, *Metal Carbonyls* (Khimiya, Moscow, 1983) [in Russian].
14. J. M. Dixon and J. E. Longfield, *Catalysis*, Vol. 7 (Reinhold, New York, 1960).
15. A. N. Zakharov, L. N. Burenkova, and V. A. Voblikova, Zh. Prikl. Khim. **62**, 2211 (1992).
16. A. N. Zakharov, A. F. Mayorova, and N. S. Perov, J. Therm. Anal. Cal. **92**, 747 (2008).
17. P. W. M. Jacobs and A. R. T. Kureishy, Trans. Farad. Soc. **68**, 551 (1962).